Available online at www.sciencedirect.com
SCIENCE DIRECT®
Advances in Space Research 36 (2005) 1579–1586
ADVANCES IN SPACE RESEARCH (a COSPAR publication)
www.elsevier.com/locate/asr

# The smallest source region of an interplanetary magnetic cloud: A mini-sigmoid

C.H. Mandrini [a,*,1], S. Pohjolainen [b], S. Dasso [a,1], L.M. Green [c], P. Démoulin [d], L. van Driel-Gesztelyi [e,f,d], C. Foley [e], C. Copperwheat [e]

[a] Instituto de Astronomía y Física del Espacio, CONICET-UBA, CC. 67, Suc. 28, 1428 Buenos Aires, Argentina
[b] Tuorla Observatory/VISPA, University of Turku, FIN-21500 Piikkiö, Finland
[c] School of Physics and Astronomy, Cardiff University, 5 The Parade, Cardiff CF24 3YB, UK
[d] Observatoire de Paris, Meudon, LESIA, UMR 8109 (CNRS), F-92195 Meudon, Cedex, France
[e] Mullard Space Science Laboratory, University College London, Holmbury St. Mary, Dorking, Surrey RH5 6NT, UK
[f] Konkoly Observatory, Budapest, Pf. 67, H-1525, Hungary

Received 20 October 2004; received in revised form 4 February 2005; accepted 4 February 2005

**Abstract**

We provide evidence for the smallest sigmoid eruption – CME – interplanetary magnetic cloud event ever observed by combining multi-wavelength remote sensing and in situ observations, as well as computing the coronal and interplanetary magnetic fields. The tiny bipole had 100 times less flux than an average active region (AR). It had a sigmoidal structure in the corona and we detected a very high level of twist in its magnetic field. On 11 May 1998, at about 8 UT, the sigmoid underwent eruption evidenced by expanding elongated EUV loops, dimmings and formation of a cusp. The Wind spacecraft, 4.5 days later, detected one of the smallest magnetic clouds (MC) ever identified (100 times less magnetic flux than an average MC). The link between the EUV bright point eruption and the interplanetary MC is supported by several pieces of evidence: timing, same coronal loop and MC orientation relative to the ecliptic, same magnetic field direction and magnetic helicity sign in the coronal loops and in the MC, comparable magnetic flux measured in the dimming regions and in the interplanetary MC and, most importantly, the pre- to post-event change of magnetic helicity in the solar corona is found to be comparable to the helicity content of the cloud.


*Keywords:* MHD and plasmas; Solar physics; Flares; Bursts and related phenomena; Interplanetary space

## 1. Introduction

In general, coronal mass ejections (CMEs) are thought to be phenomena that involve a large-scale reconfiguration of the solar corona, accompanied by significant disturbances in the solar wind. CMEs appear in the interplanetary medium as interplanetary CMEs (ICMEs). A subset of these ICMEs, called magnetic clouds (MCs), has well defined characteristics: a coherent rotation of the magnetic field vector, an enhanced field strength, as well as a proton temperature lower than in the surrounding solar wind (Burlaga et al., 1981). This subset has been thoroughly studied and there is increasing evidence that the helicity sign of MCs matches that of their solar source region (Bothmer and Schwenn, 1994; Rust, 1994; Marubashi, 1997; Yurchyshyn et al., 2001). As in the case of CMEs, most of the MC studies have focused on large scale events which last as long as a few days (see e.g., Lepping et al., 1990;

* Corresponding author. Tel.: +54 11 478 32 642; fax: +54 11 478 68 114.
*E-mail address:* mandrini@iafe.uba.ar (C.H. Mandrini).
[1] Member of the Carrera del Investigator Científico, CONICET, Argentina.

0273-1177/$30 © 2005 COSPAR. Published by Elsevier Ltd. All rights reserved.
doi:10.1016/j.asr.2005.02.003

Zhao et al., 2001). However, both at the coronal level and in the interplanetary medium much smaller events are observed as well (e.g., narrow CMEs (Munro and Sime, 1985; Howard et al., 1985), and small interplanetary flux ropes (Shimazu and Marubashi, 2000)).

During a survey of X-ray bright points (Pohjolainen, 2000) with enhanced radio emission, we found an isolated radio bright point near the centre of the disc on 11 May, 1998 (see Fig. 1, left). This structure showed signs of an eruptive nature, such as elongated sigmoidal loops which later disappeared, EUV dimmings and cusp formation (in the largest event). We describe, in Section 2, the global evolution of the small bipolar AR at the photospheric level and in the corona. Then, the coronal eruptions are analyzed in Section 3, where we quantify the amount of magnetic flux and helicity involved. In Section 4, we analyze the interplanetary data plausibly associated with this coronal ejection, and we derive the same physical quantities as at the coronal level. In Section 5, we link the events observed in the corona and the interplanetary space and we conclude.

## 2. The small bipole at different atmospheric levels

We analyze the global evolution of the X-ray flux of this bipole using Yohkoh/Soft X-ray Telescope (SXT, Tsuneta et al., 1991) full-disc images (5 arcsec per pixel). The soft X-ray light curve presents several peaks (Fig. 1, right). The most intense events are observed during 11 May. The first one lasted for ≈26 min. Two X-ray bursts followed this one. The second event occurred between 06:00 UT and 08:00 UT; while the third, which started at about 8:30 UT, had a duration of ≈3 h.

The photospheric magnetic evolution of this bipole can be followed in data obtained with the Michelson Doppler Imager (MDI, Scherrer et al., 1995) on board the Solar and Heliospheric Observatory (SOHO). We observe that the bipole orientation was changing with time (Fig. 2, top), the axis joining both polarities rotated clockwise, mostly because magnetic field elongations (that we call "tongues") are retracting. This implies a negative twist (see the Fig. 5 and corresponding discussion in López Fuentes et al., 2000). We measure the magnetic flux in the bipole, which at peak evolution was $3.2 \times 10^{20}$ Mx (average between positive and absolute value of the negative fluxes); this value puts this bipole into the 'small active region' category (Schrijver and Zwaan, 2000).

The complete evolution of the EUV emission of this small AR is best covered by data from the SOHO/Extreme-Ultraviolet Imaging Telescope (EIT, 2.6 arcsec per pixel) (Delaboudiniere et al., 1995). Globally the EUV emission followed the evolution of the photospheric magnetic field; in particular, the emission extends and rotates in parallel to the photospheric "boundary conditions" (see Fig. 2, bottom). On top of this global behaviour, there is a specific evolution of the EUV emission that is linked to the magnetic stress accumulation in the corona, and later to the global magnetic instability (see Section 3.1).

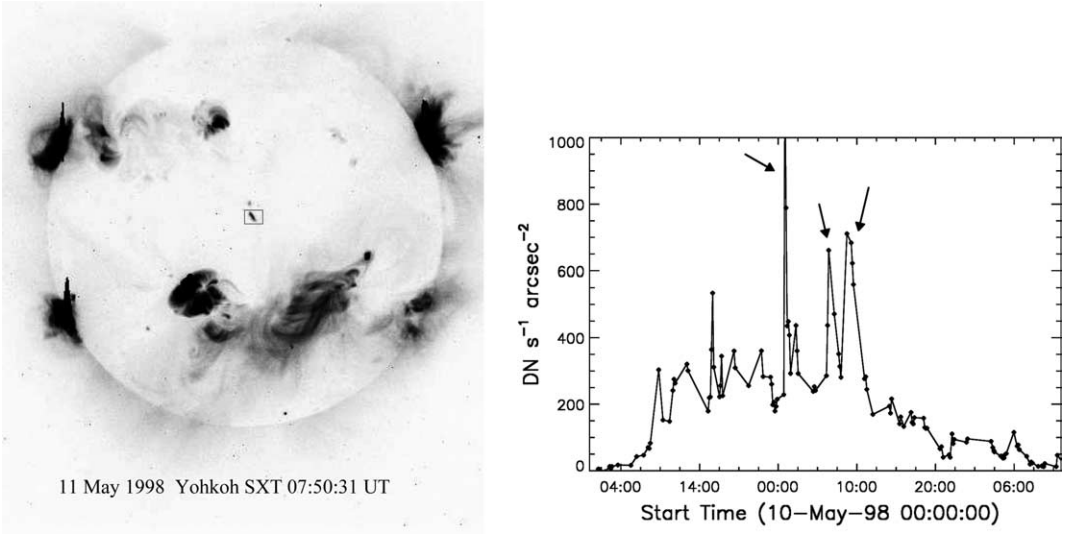


Fig. 1. SXT full disc image (left) and flux evolution (right) from the emergence to the disappearance of the small AR. The image corresponds to the time of maximum extension of the X-ray bright point (shown within the box), which is located very far from other ARs. The X-ray flux curve was obtained using the software SXT_FLUX with a fixed temperature of 2 MK, determined using the thin Aluminum (Al.1) and the Dagwood filters (Al–Mg). This program, from the Yohkoh software package, computes DN/s given the temperature and the filter, the DN/s values were calculated over the area covered by the small bright point and then divided by this area in arcsec$^2$. Three main bursts can be seen in X-rays (marked with arrows), all occurred on 11 May: the first at ~01:00 UT, the second at ~07:00 UT, and the third at ~08:30 UT.

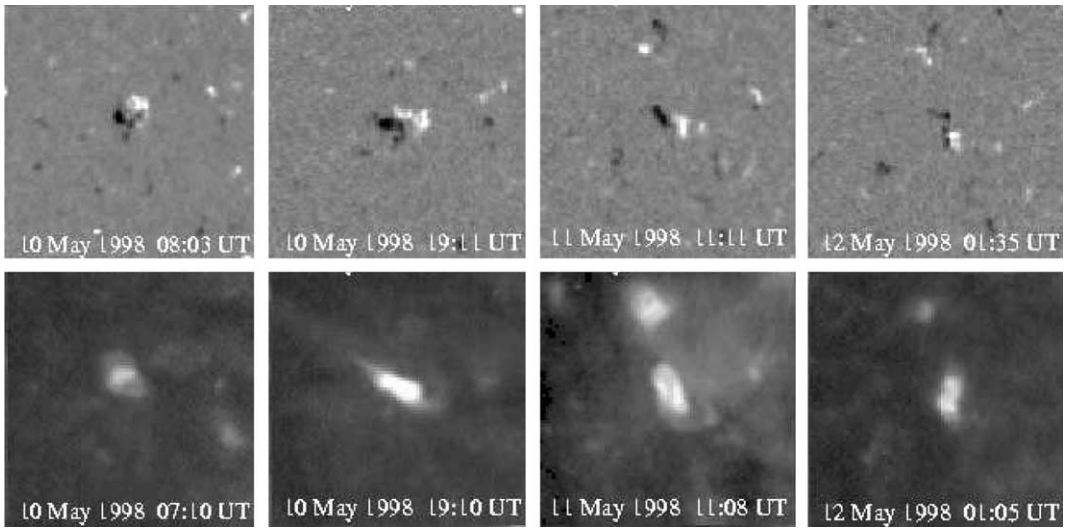


Fig. 2. Photospheric magnetograms from SOHO/MDI (top) and EUV images from SOHO/EIT (bottom). Both sets of images show the evolution of the bright point region from 10 to 12 May, 1998, with a field of view of 200 × 200 arcsec (1.98 arcsec per pixel). The maps have been coaligned and de-rotated to central meridian position (11 May 04:15 UT). All the EIT images shown are taken with the 284 Å filter, except the one on 11 May at 11:08 UT where the wavelength is 195 Å.

## 3. The coronal eruptions

### 3.1. Observational evidences

Dimmings are often observed in connection with eruptive events (Sterling and Hudson, 1997; Zarro et al., 1999; Thompson et al., 2000). In the case studied here, EUV dimmings were clearly observed associated with the first and third X-ray events. The top row of images in Fig. 3 illustrates the first event. At 00:35 UT the bright point is relatively intense and elongated. After the X-ray burst occurs, the shape becomes roundish. A dimming region is observed extending towards the North-East, while no reduced emission appears to the South-West. For the third burst, the image at 08:31 UT shows the erupting loops and an elongated

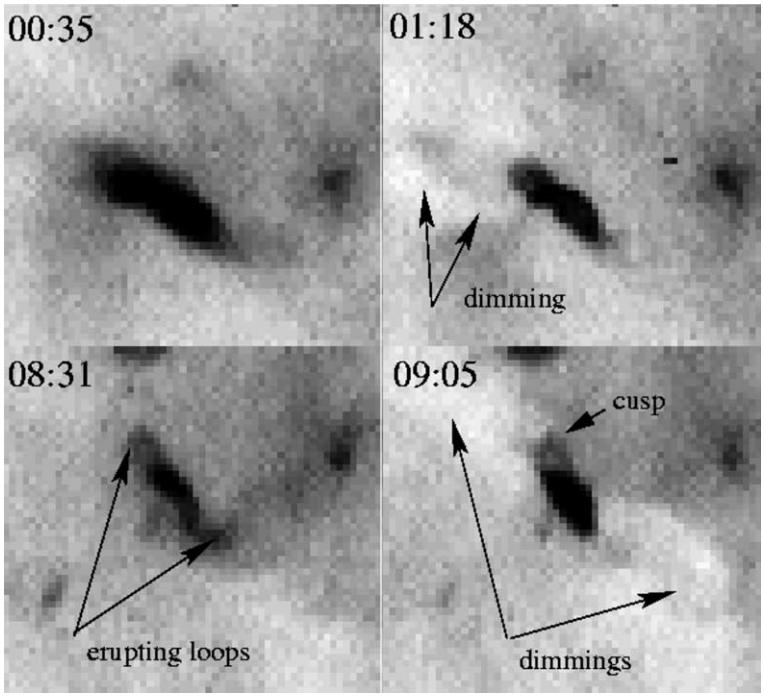


Fig. 3. EIT 195 Å images in contrast-enhanced reversed grey levels (enhanced emission in black, reduced in white) of the bright point during the first and third X-ray bursts indicated in Fig. 1, right.

bright core. At 09:05 UT, the dimmings are well defined, the central brightening becomes compact and a cusp structure has formed above the bright point. This third event is the largest in terms of integrated X-ray flux, EUV intensity and area of EUV dimmings. In what follows we will concentrate only on the third, and largest, event.

### 3.2. Computation of global physical quantities

The magnetic flux contained in a solar ejecta is an important global quantity that can be used to link the coronal observations to the interplanetary ones. An upper limit to this quantity can be estimated considering the magnetic flux contained in the dimmings. The dimmings after the third event cover both part of the small AR polarities and the surrounding quiet Sun regions. We have computed the magnetic flux in the dimmings above the AR bipole, $F_{\mathrm{AR,dimming}} = 12 \pm 2 \times 10^{19}$ Mx (the error comes from the uncertainty in the determination of the dimming boundaries). This flux, computed separately for the positive and negative polarities, is almost balanced and is about 60% of the magnetic flux present in each polarity at the same time. Since in the dimmed quiet Sun areas we mainly find weak-field polarities, whose flux is not associated to the "open" flux in the ejecta, we chose to compute the net flux only in those pixels with values above a given threshold (we selected different threshold values between 0 and 50 G). We find that the net flux (difference between positive and negative flux in each lobe) in the dimmings above the quiet solar regions is small, $\approx$0.5 up to $1.0 \times 10^{19}$ Mx, in the range of the selected thresholds. This is less than 8% of the flux in the dimmings over the small AR. Then, the total net flux in the dimmings (quiet Sun regions and part of AR polarities) is $F_{\mathrm{dimming}} = 13 \pm 2 \times 10^{19}$ Mx.

Another important physical quantity to link coronal observations to interplanetary ones is the magnetic helicity, because it is nearly conserved both in the corona and the heliosphere. To compute this quantity we need first to model the coronal magnetic field. Using MDI magnetograms, we have extrapolated the observed photospheric line of sight component of the field to the corona under the linear (or constant $\alpha$) force-free field assumption: $\vec{\nabla} \times \vec{B} = \alpha \vec{B}$. The value of $\alpha$ is chosen so as to best fit the observed coronal loops observed with the Transition Region and Coronal Explorer (TRACE, Handy et al., 1999, see Fig. 4). As usually found before in other ARs, $\alpha$ is higher in the core of the region $\alpha = -0.11$ Mm$^{-1}$ (thick lines in Fig. 4) than in the peripheries $\alpha = -0.08$ Mm$^{-1}$ (thin lines). Having the model, we compute the relative coronal magnetic helicity, $H_{\mathrm{cor}}$, using a linearized expression of Eq. A23 in Berger (1985), as discussed by Green et al. (2002) (see their Eq. 11; notice that the factor 2 in front of $\alpha$ is a typographic error and should be omitted; however, this typo is only present in the script and did not influence the results).

When a flux tube is ejected from the solar corona into the interplanetary medium, it carries part of the magnetic helicity contained in the coronal field. Therefore, we need to compute the variation of the coronal magnetic helicity before and after an eruptive event to compare this coronal global quantity to the corresponding one in the associated interplanetary event. Unfortunately, TRACE images are only available dur-

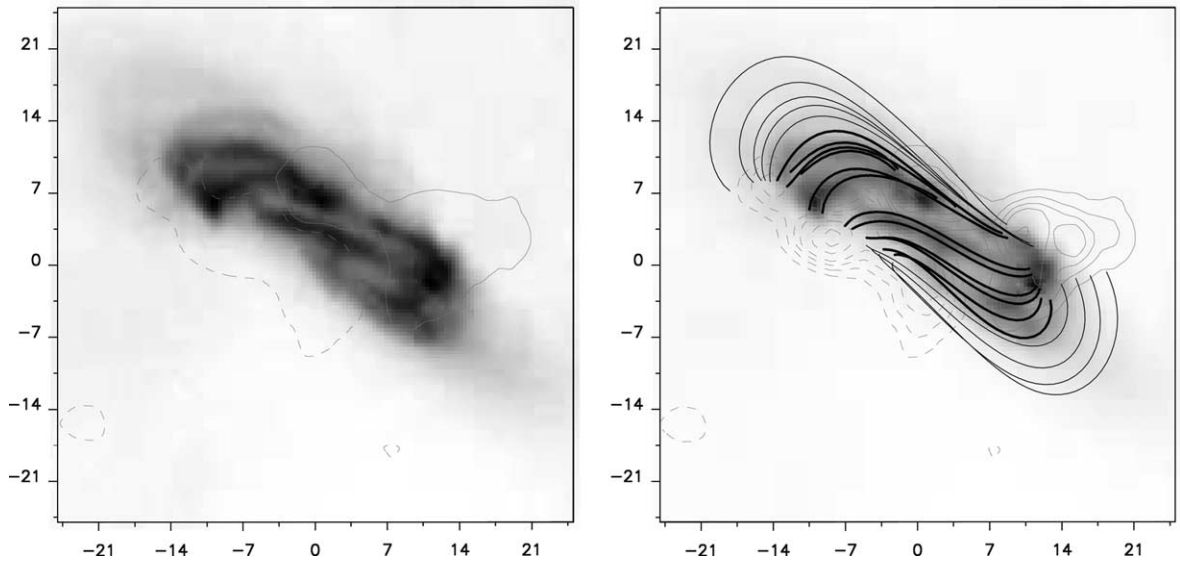


Fig. 4. TRACE 195 Å observation (left) and coronal magnetic field model (right). Two isocontours (±25 G, grey lines) of the photospheric field taken with MDI at 00:03 UT (positive, continuous; negative, dashed) overlaid the TRACE image taken at 00:38 UT (0.5 arcsec per pixel). On the right we show the same image with more magnetic isocontours (±25, 50, 75, 100, 150, 200 G, grey lines) and computed field lines superimposed (the thin lines correspond to $\alpha = -0.08$ Mm$^{-1}$ and the thick lines to $\alpha = -0.11$ Mm$^{-1}$).

Table 1
Left block of columns shows the time, the range of the linear force-free field parameter $\alpha$, and the range of the AR relative magnetic helicity, $H_{cor}$

| Active region | | | Magnetic cloud | | |
|---|---|---|---|---|---|
| Time (UT) | $\alpha$ ($Mm^{-1}$) | $H_{cor}$ ($10^{39}$ $Mx^2$) | $F_z$ ($10^{19}$ Mx) | $F_\phi/L$ ($10^{19}$ Mx/AU) | $H_{MC}/L$ ($10^{39}$ $Mx^2$/AU) |
| 00:03 | −0.08/−0.11 | −5.2/−7.5 | 1.3 | 20. | −3.0 |
| 11:11 | −0.08/−0.11 | −2.9/−4.2 | | | |

The right block shows the flux of the $B_z$ component ($F_z$) and of the $B_\phi$ component ($F_\phi$), and the relative magnetic helicity per unit length, $H_{MC}/L$, for the small related magnetic cloud using Lundquist's model.

ing a short period of time before the first X-ray burst. Furthermore, due to the low intensity and spatial resolution of both SXT and even EIT, it is difficult to recognize the shape of individual coronal loops and to use their images to determine the value of $\alpha$. Therefore, taking a conservative approach to determine a lower bound for the variation of the coronal magnetic helicity, we use the MDI magnetogram after the third X-ray burst (11:11 UT) and the previously determined values for $\alpha$ to compute $H_{cor}$ at that time. Our results are shown in Table 1. The magnetic helicity change in the corona before and after the event is $2.3\times10^{39}$ $Mx^2 \leqslant |\Delta H_{cor}| \leqslant 3.3\times10^{39}$ $Mx^2$.

## 4. The small interplanetary magnetic cloud

### 4.1. Observational evidences

We analyze interplanetary data around the expected time of arrival (2–5 days after the coronal event) with the hope to identify the interplanetary manifestation of the strongest sigmoidal eruption (third X-ray burst). From ~10:00 UT on 13 May to ~04:00 UT on 16 May, the spacecraft Wind (located in the vicinity of the Lagrangian point, LI) observed low values of the radial velocity ($V_r$) of the solar wind (300 km/s $\leqslant |V_r| \leqslant$ 400 km/s). A very extended region containing plasma of a low proton $\beta$ (being $\beta$ the ratio of the plasma to the magnetic pressure) and a disordered high intensity magnetic field, was observed between 15 and 17 May, 1998. These are considered signatures of complex interplanetary ejecta. We found that the duration of the complex ejecta is around 50 h in 1 min resolution Wind data, which were downloaded from http://cdaweb.gsfc.nasa.gov/cdaweb/istp-public/. By scanning the full temporal evolution of the ejecta and separating the data in different sections, we are able to isolate a small event, having the characteristics of a magnetic cloud, that lasted from 22:00 UT on 15 May to 01:50 UT on 16 May, about 4 days and 14 h (110 h) after the sigmoidal eruption. Considering an average speed of ~350 ± 50 km/s (the mean observed speed of the solar wind), we expect a travel time of ~119 ± 17 h from the Sun to 1 AU; then, the small event is a good candidate to be the interplanetary manifestation of the coronal eruption.

### 4.2. Magnetic cloud model and global physical quantities

To determine the orientation of the cloud we apply the standard minimum variance (MV) method to the data (see e.g. Bothmer and Schwenn, 1998). With the definition of the orientation angles $\theta$ and $\varphi$ as in Dasso et al. (2003), we find that $\theta \sim 59°$ and $\varphi \sim 172°$, so the projection of the axis of the cloud on the ecliptic plane lies almost along $\hat{x}_{GSE}$ (the $x$ coordinate in the Geocentric Solar Ecliptic system). In this approach the spacecraft impact parameter, $p$, is not determined and we set it equal to zero, noting that the large angle rotation of the field (~147°) indicates that the ratio between the closest distance approach to the MC centre and the radius of the cloud ($p$) should be small. Then, we obtain the components of the field in the local cartesian system of coordinates, such that: (a) $B_{z,cloud}$ is the axial component, its value being positive at the cloud centre, (b) $B_{y,cloud}$ is the azimuthal component once the spacecraft crossed the MC axis ($p = 0$), and (c) $B_{x,cloud}$ is the radial component, also after leaving the MC centre.

Several models and fitting methods have been used to reproduce the magnetic structure of MCs (see e.g., Dasso et al., 2003); however, it is not yet clear which one is the best to describe it. We model the small cloud field considering a linear force-free field configuration (Lundquist, 1950), which is the most frequently used (two other models were used as well in Mandrini et al., 2005, giving similar results). The physical parameters that fit best the observations are computed following the method described in Dasso et al. (2003). The radius of the cloud ($R = 1.6\times10^{-2}$ AU) is estimated from the duration of the MC and the observed solar wind speed. The observations and the fitted curves are shown in Fig. 5 for $B_{z,cloud}$ and $B_{y,cloud}$ ($|B_{x,cloud}| \ll |B_{y,cloud}|$, $|B_{z,cloud}|$).

We next compute some global quantities to be compared to the corresponding coronal ones. An expression for the gauge-invariant relative magnetic helicity per unit length ($H_{MC}/L$) has been deduced by Dasso et al. (2003) for the model used here. We compute the magnetic flux ($F_{z,cloud}$) of $B_{z,cloud}$ (i.e., along the flux tube) and the magnetic flux ($F_{\phi,cloud}/L = \int_0^R \mathrm{d}r B_\phi(r)$) of $B_{\phi,cloud}$ (i.e., across a section of the cloud containing its axis). Our results are shown in Table 1.

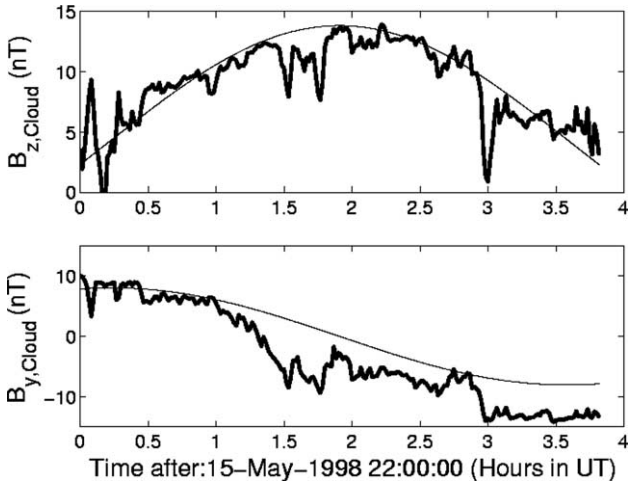


Fig. 5. Magnetic field components in the local MC coordinates. We show the evolution of the axial ($B_{z,\mathrm{cloud}}$) and azimuthal ($B_{y,\mathrm{cloud}}$) magnetic field components (with the orientation of the cloud given by the MV method and with a null impact parameter). The observed magnetic data are drawn with thick lines and the best solutions, fitted using Lundquist's model, with thin lines.

## 5. The link between the coronal eruption and the magnetic cloud

The small AR at disc centre on 11 May 1998 produced three main X-ray bursts. The third one was the most significant in X-ray total flux, in EUV evolution and also in signatures of eruption. This coronal eruption and the interplanetary MC, described in Section 4, have properties that indicate their association, such as:

(a) The location, i.e., the eruption occurred very close to the disc centre and, since the ejections travel dominantly in the radial direction, this implies that the resulting MC has a chance to be observed by Wind.
(b) The timing, i.e., 4.5 days travel time is expected for a slow CME moving at the speed measured by Wind (≈ the slow solar wind speed, e.g., Vršnak and Gopalswamy, 2002).
(c) The spatial orientation, i.e., the MC axis is oriented in almost the same direction as that of the elongated coronal sigmoid.
(d) The signs of the axial magnetic field of the MC and of the AR polarities and of the helicities agree.

Since the probability that all these characteristics match merely by pure chance is very low, we conclude that the observed small MC is most probably the consequence of the observed coronal eruption. We summarize our view in Fig. 6, where we indicated that the Wind spacecraft probably crossed the positive (western) leg of the flux rope (as can be deduced from the interplanetary magnetic field, the orientation of the MC and the geometry of the coronal magnetic field).

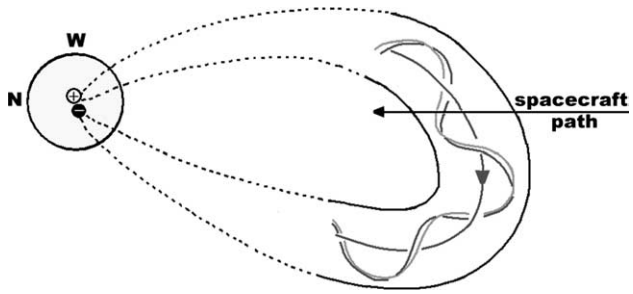


Fig. 6. Schematic global view of the magnetic cloud and its source region (solar North is to the left). The MC leading part is represented by continuous lines, while dashed lines are used closer to the Sun since, considering the photospheric magnetic observations, the MC could be detached from its solar source by the time it was observed by Wind.

We now attempt to quantify this link through the measured magnetic fluxes and calculated helicities. To compare the coronal and interplanetary magnetic helicities, the main unknown is the distribution of the twist along the flux rope. But even assuming a uniform distribution, the length remains unknown. For the studied MC, we know that the photospheric magnetic bipole disappeared about one day after the eruption (Fig. 2, last top image), so we assume that the erupting flux rope has to be detached from its original solar source by the time it was observed by Wind. With a simple proportionality we find a length of ≈0.5 AU. However, since after reconnection with large-scale field lines the magnetic twist contained in the ejected flux tube should propagate along the new magnetic connectivities as a torsional Alfvén wave, we can add a flux rope length of 0.2 AU at both ends of the tube (using a time period of 3.5 days and a typical Alfvén velocity of 100 km s$^{-1}$). Then, we conclude that the most likely length of the observed MC is between 0.5 and 1 AU. Therefore, the estimated cloud helicity is $|H_{\mathrm{MC}}| \approx 1.5\text{–}3 \times 10^{39}$ Mx$^2$, being in good agreement with the decrease of the magnetic helicity in the corona, $2.3 \times 10^{39}\ \mathrm{Mx}^2 \leqslant |\Delta H_{\mathrm{cor}}| \leqslant 3.3 \times 10^{39}\ \mathrm{Mx}^2$ (Table 1).

The magnetic flux computed in the dimming regions was $F_{\mathrm{dimming}} = 13 \pm 2 \times 10^{19}$ Mx. Which of the two flux values ($F_z$ or $F_\phi$) computed for the MC should this value be compared to? If the MC would result from a simple expansion of coronal loops, then $F_{\mathrm{dimming}}$ corresponds to the flux of the axial field component of the MC. However, in our case, $F_z$ is only one tenth of $F_{\mathrm{dimming}}$. If the ejection were the result of the expulsion of a twisted flux tube formed during the eruption by successive reconnections in a sheared magnetic arcade, which we think is our case; then, $F_{\mathrm{dimming}}$ should be closer to the value of the flux in the azimuthal component of the cloud. Considering a length between 0.5 and 1 AU for the cloud, we find the flux $10 \times 10^{19}\ \mathrm{Mx} \leqslant F_\phi \leqslant 20 \times 10^{19}$ Mx, in quite good agreement with $F_{\mathrm{dimming}}$.

From the common properties between the magnetic configuration in the corona (sigmoidal bright point)

and the interplanetary space (small MC), but also from finding comparable magnetic fluxes and helicities in them, we conclude that the observed coronal eruption (third X-ray burst) indeed resulted in the small MC. These small events not only present a challenge for present CME theoretical models, which are developed for large scale magnetic configurations, but also broaden our knowledge about the range of physical parameters where a CME can occur. Both high non-potentiality in the active region and weak overlying stabilizing magnetic field (the quiet Sun environment) seem to be important factors in reaching a successful eruption (Török and Kliem, 2004). To understand better this kind of small events, we need coronal observations with both a better sensitivity (dynamic range) and spatial resolution. The next missions, Solar B and Solar Orbiter, will greatly contribute to this kind of research. Furthermore, to observe the associated halo CME is a challenge. STEREO, with its two satellite configuration, will allow us to observe events from a lateral point of view from which it will be easier to detect the scattered light of such a small CME.

## Acknowledgments

The authors thank the TRACE, WIND, SOHO/MDI and EIT consortia for their data, and the Mullard Space Science Laboratory (MSSL) Solar UK Research Facility (SURF) for YOHKOH/SXT. SOHO is a joint project by ESA and NASA. S.P. acknowledges a joint travel grant from CIMO (Finland) and EGIDE (France). P.D. and C.H.M. acknowledge financial support from ECOS (France) and SECyT (Argentina) through their cooperative science program (A01U04). C.H.M. and L.v.D.G. thank TET (Hungary) and SECyT for financial support through their cooperation program (AR03/02 and HU/A01/UIII/01). P.D. and L.v.D.G. acknowledge travel support from the Royal Society Joint Project (MSSL/UCL-Observatoire de Paris, Meudon). C.H.M. thanks COSPAR for a travel grant. C.H.M. and S.D. thank support from the Argentinean Grants UBACyT X329, CONICET PIPs 2388–2693 and ANPCYT PICT-12187. L.v.D.G. was supported by the Hungarian Government Grant OTKA T-038013.

## References

Berger, M.A. Structure and stability of constant-alpha force-free fields. Astrophys. J. Sup. Ser. 59, 433–444, 1985.

Bothmer, V., Schwenn, R. Eruptive prominences as sources of magnetic clouds in the solar wind. Space Sci. Rev. 70, 215, 1994.

Bothmer, V., Schwenn, R. The structure and origin of magnetic clouds in the solar wind. Ann. Geophys. 16, 1–24, 1998.

Burlaga, L., Sittler, E., Mariani, F., Schwenn, R. Magnetic loop behind an interplanetary shock – Voyager, Helios, and IMP 8 observations. J. Geophys. Res. 86, 6673–6684, 1981.

Dasso, S., Mandrini, C.H., Démoulin, P., Farrugia, C.J. Magnetic helicity analysis of an interplanetary twisted flux tube. J. Geophys. Res. (Space Physics) 108, 1362, doi:10.1029/2003SA009942, 2003.

Delaboudiniere, J.-P., Artzner, G.E., Brunaud, J., Gabriel, A.H., Hochedez, J.F., Millier, F., Song, X.Y., Au, B., Dere, K.P., Howard, R.A., Kreplin, R., Michels, D.J., Moses, J.D., Defise, J.M., Jamar, C., Rochus, P., Chauvineau, J.P., Marioge, J.P., Catura, R.C., Lemen, J.R., Shing, L., Stern, R.A., Gurman, J.B., Neupert, W.M., Maucherat, A., Clette, F., Cugnon, P., van Dessel, E.L. EIT: extreme-ultraviolet imaging telescope for the SOHO mission. Solar Phys. 162, 291–312, 1995.

Green, L.M., López Fentes, M.C., Mandrini, C.H., Démoulin, P., Van DrielGesztelyi, L., Culhane, J.L. The magnetic helicity budget of a CME-prolific active region. Solar Phys. 208, 43–68, 2002.

Handy, B.N., Acton, L.W., Kankelborg, C.C., et al. The transition region and coronal explorer. Solar Phys. 187, 229–260, 1999.

Howard, R.A., Sheeley, N.R., Michels, D.J., Koomen, M.J. Coronal mass ejections – 1979–1981. J. Geophys. Res. 90, 8173–8191, 1985.

López Fuentes, M.C., Démoulin, P., Mandrini, C.H., van Driel-Gesztelyi, L. The counterkink rotation of a non-Hale active region. Astrophys. J. 544, 540–549, 2000.

Lepping, R.P., Burlaga, L.F., Jones, J.A. Magnetic field structure of interplanetary magnetic clouds at 1 AU. J. Geophys. Res. 95, 11957–11965, 1990.

Lundquist, S. Magnetohydrostatic fields. Ark. Fys. 2, 361–365, 1950.

Mandrini, C., Pohjolainen, S., Dasso, S., Green, L., Démoulin, P., van Driel-Gesztelyi, L., Copperwheat, C., Foley, C. Interplanetary flux rope ejected from an X-ray bright point. Astron. Astrophys., 2005, in press.

Marubashi, K. In: Coronal Mass Ejections, Geophysical Monograph 99. p. 147, 1997.

Munro, R.H., Sime, D.G. White-light coronal transients observed from SKYLAB May 1973 to February 1974 – a classification by apparent morphology. Solar Phys. 97, 191–201, 1985.

Pohjolainen, S. On the origin of polar radio brightenings at short millimeter wavelengths. Astron. Astrophys. 361, 349–358, 2000.

Rust, D.M. Spawning and shedding helical magnetic fields in the solar atmosphere. Geophys. Res. Lett. 21, 241–244, 1994.

Scherrer, P.H., Bogart, R.S., Bush, R.L., Hoeksema, J.T., Kosovichev, A.G., Schou, J., Rosenberg, W., Springer, L., Tarbell, T.D., Title, A., Wolfson, C.J., Zayer, L.MDI Engineering Team The solar oscillations investigation - Michelson Doppler imager. Solar Phys. 162, 129–188, 1995.

Schrijver, C.J., Zwaan, C. Solar and Stellar Magnetic Activity. Cambridge University Press, NewYork, (Cambridge Astrophysics Series 34), 2000.

Shimazu, H., Marubashi, K. New method for detecting interplanetary flux ropes. J. Geophys. Res. 105, 2365–2374, 2000.

Sterling, A.O., Hudson, H.S. YOHKOH/SXT observations of X-ray "dimming" associated with a halo Coronal Mass Ejection. Astrophys. J. Lett. 491, L55, 1997.

Török, T., Kliem, B. The kink instability of a coronal magnetic loop as a trigger mechanism for solar eruptions. Publications of the Astronomy Deparment of the Eotvos Lorand University, Lorand, vol. 14. pp. 165–176, 2004.

Thompson, B.J., Cliver, E.W., Nitta, N., Delannée, C., Delaboudiniére, J.P. Coronal dimmings and energetic CMEs in April–May 1998. Geophys. Res. Lett. 27, 1431–1434, 2000.

Tsuneta, S., Acton, L., Bruner, M., Lemen, J., Brown, W., Caravalho, R., Catura, R., Freeland, S., Jurcevich, B., Owens, J. The soft X-ray telescope for the SOLAR-A mission. Solar Phys. 136, 37–67, 1991.

Vršnak, B., Gopalswamy, N. Influence of the aerodynamic drag on the motion of interplanetary ejecta. Journal of Geophys. Res. (Space Physics) 107, 1019, doi:10.1029/2001JA000120, 2002.

Yurchyshyn, V.B., Wang, H., Goode, P.R., Deng, Y. Orientation of the magnetic fields in interplanetary flux ropes and solar filaments. Astrophys. J. 563, 381–388, 2001.

Zarro, D.M., Sterling, A.C., Thompson, B.J., Hudson, H.S., Nitta, N. SOHO EIT Observations of Extreme-Ultraviolet ''Dimming'' Associated with a Halo Coronal Mass Ejection. Astrophys. J. Lett. 520, L139–L142, 1999.

Zhao, X.P., Hoeksema, J.T., Marubashi, K. Magnetic cloud Bs events and their dependence on cloud parameters. Journal of Geophys. Res. 106, 15643–15656, 2001.